PCCP

Cite this: *Phys. Chem. Chem. Phys.*, 2012, **14**, 11441–11447

www.rsc.org/pccp

PAPER

1*H*-1,2,4-Triazole as solvent for imidazolium methanesulfonate

Jiangshui Luo,[ab] Tran Van Tan,[c] Olaf Conrad*[d] and Ivo F. J. Vankelecom*[a]

Received 5th April 2012, Accepted 13th June 2012
DOI: 10.1039/c2cp41098b

The solvation effect of 1*H*-1,2,4-triazole towards imidazolium methanesulfonate was studied by blending imidazolium methanesulfonate and 1*H*-1,2,4-triazole. Upon addition of 1*H*-1,2,4-triazole, the melting point of imidazolium methanesulfonate was lowered to less than 100 °C while maintaining the high ionic conductivity for a wide composition range of the blend. The ionic conductivity of the blend can be adequately described by using the Vogel–Fulcher–Tamman equation. A vehicle mechanism is postulated to govern the proton conduction for the blend. The contribution of protons to the ionic conductivity was corroborated electrochemically. The blend exhibited electrochemical activities for H_2 oxidation and O_2 reduction at a Pt electrode, as well as a wide electrochemical window. Therefore, suitable blends can possibly serve as electrolytes for polymer electrolyte membrane fuel cells operating under non-humidifying conditions. The solvation effect studied herein suggests a promising approach to a wider application area of protic ionic liquids.

1. Introduction

Protic ionic liquids (PILs), formed by the stoichiometric combination of a Brønsted acid and a Brønsted base, have been intensively studied in various fields such as organic synthesis, catalysis, and polymer electrolyte membrane fuel cells (PEMFCs), due to their many beneficial properties.[1–10]† However, the reported PILs often have relatively high melting points,[1–8] hindering their further applications as electrolytes in spite of their favorable properties such as high ionic conductivity and good thermal stability.

PILs dissolved in organic solvents, such as Brønsted bases,[7–12] acetonitrile,[13,14] alcohols,[14,15] and even salts,[5b,c] show some interesting characteristics. Very recently, the solution of tributylphosphonium tetrafluoroborate in acetonitrile was used as an electrolyte for carbon-based supercapacitors, resulting in capacities comparable to conventional aqueous electrolytes.[13] Moreover, eutectic solutions of binary guanidinium salts, with eutectic temperatures much lower than both of the individual salts, showed aqueous solution-like ionic conductivities.[5c] Particularly, the limited available reports on PILs dissolved in Brønsted bases are essentially nonstoichiometric acid–base combinations, wherein the PILs are prepared from the same Brønsted bases as the solvents.[7–12] In these systems, the ionic conductivity was often observed to reach a maximum in the base-rich compositions. It has been argued that the Brønsted bases, for example, imidazole or 1*H*-1,2,4-triazole, accelerate proton transfer mainly *via* the Grotthuss mechanism and thus actually act as proton solvents.[11,12]

Imidazole and 1*H*-1,2,4-triazole are two typical Brønsted bases. Both of them have a similar molecular structure and a similar high boiling point. Imidazole (pK_{a1} = 6.99, pK_{a2} = 14.44) has much more basic character than 1*H*-1,2,4-triazole (pK_{a1} = 2.27, pK_{a2} = 10.26),[16] implying that the basic nitrogen of 1*H*-1,2,4-triazole may have lower electron density[11] and lower proton affinity[17] than its imidazole counterpart. Importantly, 1*H*-1,2,4-triazole has adequate electrochemical stability under fuel cell conditions[8,11] and was reported to be an ideal solvent to promote proton conductivity of materials at temperatures above 100 °C.[11] To better understand the role of the Brønsted base in a base-rich blend, it would be beneficial to explore a PIL prepared from a stronger Brønsted base (*e.g.* imidazole) and dissolved in the weaker Brønsted base 1*H*-1,2,4-triazole. Angell *et al.*[18a] described that imidazole-doped ethylammonium hydrogensulfate yielded behavior superior in all respects to that of the industry standard phosphoric acid electrolyte. However, detailed knowledge of the physicochemical properties, especially electrochemical behavior, of the mixture of a PIL and a Brønsted base, whose pK_a value is intermediate between

[a] *Centre for Surface Chemistry and Catalysis, Faculty of Bioscience Engineering, KU Leuven, Kasteelpark Arenberg 23, Box 2461, Leuven, 3001, Belgium. E-mail: ivo.vankelecom@biw.kuleuven.be; Fax: +32 16 321998; Tel: +32 16 321594*
[b] *NEXT ENERGY · EWE-Forschungszentrum für Energietechnologie e.V., Carl-von-Ossietzky-Str. 15, D-26129 Oldenburg, Germany*
[c] *Quantum Chemistry and Physical Chemistry Section, Department of Chemistry, KU Leuven, Celestijnenlaan 200F, Box 2404, B-3001, Leuven, Belgium*
[d] *HySA/Catalysis, Dept. of Chemical Engineering, University of Cape Town, Private Bag X3, Rondebosch, Cape Town, 7701, South Africa. E-mail: olaf.conrad@uct.ac.za; Tel: +27 21 650 4366*

† Although the melting points of the protic salts should be lower than 100 °C to qualify the liquids as protic ionic liquids (PILs) by the familiar criterion, PILs are used here to refer to all protic molten salts for convenience.

that of the acid and the base of the PIL, is still very limited.[18a]

In this paper, in order to develop suitable electrolytes for medium temperature PEMFCs under non-humidifying conditions, we studied the physicochemical properties of imidazolium methanesulfonate dissolved in 1*H*-1,2,4-triazole. Unlike in previously studied similar systems,[7–12] we could not find evidence that 1*H*-1,2,4-triazole functions as a proton solvent in our system. However, it dramatically lowered the melting temperature while maintaining the high ionic conductivity of imidazolium methanesulfonate, indicating that it may act as an effective solvent to dissolve and dissociate the PIL. Particularly, similar to the deep eutectic solvent of choline chloride and urea reported by Abbott *et al.*,[18b,c] a eutectic mixture was found when the mole ratio for imidazolium methanesulfonate *vs.* 1*H*-1,2,4-triazole was 1 : 3. The proton conduction was confirmed by chronoamperometry under a H_2 atmosphere. Moreover, the electrochemical activity and stability of the mixture have been evaluated *via* cyclic voltammetry and linear sweep voltammetry. Our results suggest a practical and generalized approach for utilizing the PILs with high melting temperatures in devising proton conductors under non-humidifying conditions.

2. Experimental

2.1 Chemicals

Equimolar amounts of imidazole ($C_3H_4N_2$, Sigma-Aldrich, $\geq$ 99.5%) and methanesulfonic acid (CH_3SO_3H, Sigma-Aldrich, $\geq$ 99.5%) were weighed in a UniLab glove box (MBRAUN) with pure N_2 atmosphere (water content $<$0.1 ppm) and then mixed together, followed by heating above the melting point to promote the formation of the protic salt imidazolium methanesulfonate ($C_3H_5N_2^+ \cdot CH_3SO_3^-$ (**1**)). Appropriate amounts of 1*H*-1,2,4-triazole ($C_2H_3N_3$ (**2**), Acros Organics, 99.5%) were added into **1** and then heated above the respective melting points with stirring, resulting in transparent and homogeneous compositions with different mole ratios for **1** *vs.* **2**: n_1/n_2 = 2/1, n_1/n_2 = 3/4, n_1/n_2 = 1/3, and n_1/n_2 = 1/8, respectively. All samples were stored in the glove box. Prior to the synthesis, the water contents of imidazole, **2** and methanesulfonic acid were determined to be less than 1000 ppm, 2050 ppm and 2700 ppm, respectively, using a coulometric Karl Fischer moisture titrator (Model CA-200, Mitsubishi Chemical Analytech).

2.2 Anion concentrations

The $CH_3SO_3^-$ concentration and anion impurities such as halide and sulfate ions in **1** were determined by ion chromatography. Experimental details of the ion chromatographic analysis have been described in ref. 8.

2.3 X-ray diffraction (XRD)

Powder XRD measurements were performed for **1**, **2** and the composition of n_1/n_2 = 1/3 on a powder X-ray diffractometer (X'Pert PRO, PANalytical) using Cu Kα radiation (λ = 1.5406 Å) at room temperature.

2.4 Thermal analysis

Thermogravimetric analysis (TGA) for an approximate sample weight of 15 mg heated at 1 K min^{-1} was performed on a thermogravimetric analyzer (TGA 4000, PerkinElmer) in a stream of N_2 (30 mL min^{-1}) with open Al_2O_3 pans.

Differential scanning calorimetry (DSC) measurements were conducted on a Netzsch DSC 204 *F1 Phoenix* apparatus under a N_2 atmosphere. Samples with approximately 10 mg each were tightly sealed in Al pans. The melting temperature (T_m, onset temperature of the corresponding endothermic peak) and the eutectic temperature (T_e, peak temperature of the related endothermic peak) were determined from the DSC thermograms recorded at 10 K min^{-1} from 20 °C to 200 °C.

2.5 Fourier transform infrared (FT-IR) spectra

The FT-IR spectra were recorded at room temperature in the range of 4000–650 cm^{-1} on a PerkinElmer Spectrum 100 FT-IR spectrometer with universal ATR accessory (crystal: diamond/ZnSe) and were accumulated for 10 scans at a resolution of 4 cm^{-1}.

2.6 Ionic conductivity

The temperature dependence of the ionic conductivity for each composition in liquid state was measured from low temperature to high temperature by complex impedance spectroscopy using a platinized conductivity cell (model 6.0908.110, Metrohm) and a Solartron 1255B Frequency Response Analyzer combined with a Solartron 1287 Electrochemical Interface. The temperature was controlled at 10 K interval (±0.01 K), except for **1** whose temperature interval was 2 K (±0.01 K) starting from 192 °C to 200 °C. Test details are described in our previous work.[8]

2.7 Electrochemical polarization

Electrochemical characterizations for the n_1/n_2 = 1/3 composition were carried out at 150 °C with a three-electrode system using a Solartron 1287 Electrochemical Interface linked to a computer and monitored by the CorrWare® (Scribner Associates) software. The working electrode (WE) was a 1 mm diameter Pt wire (Radiometer Analytical) and the counter electrode (CE) an 8 mm × 8 mm Pt plate (Radiometer Analytical). The reference electrode (RE) was a 10 mm diameter Pt disk (Radiometer Analytical) immersed in the testing composition with continuous H_2 bubbling as a reversible hydrogen electrode (RHE) and was placed close to the WE through a Luggin capillary. The surface area of the WE was estimated from the hydrogen desorption peak of the cyclic voltammogram measured in 0.5 mol L^{-1} H_2SO_4 solution at room temperature. The electrodes were electrochemically cleaned by cycling in H_2SO_4 solution prior to measurements. The temperature was regulated by using a silicon oil bath.

Chronoamperograms were obtained with WE under a dry N_2 or H_2 gas bubbling atmosphere to confirm the contribution of protons to the ionic conductivity.[19] H_2 flow rate for WE was about 3 mL min^{-1}. A constant DC voltage of 500 mV was applied on WE *vs.* open circuit potential for chronoamperometric measurements.

Cyclic voltammograms were recorded at a scan rate of 20 mV s^{-1} with WE under dry N_2, H_2, or O_2 gas bubbling atmosphere, respectively. H_2 and O_2 flow rates were both about 3 mL min^{-1}.

Electrochemical stability was analyzed with linear sweep voltammetry recorded at 10 mV s^{-1}. Both the WE and the CE were in dry N_2 sparged electrolyte.

3. Results and discussion

3.1 Anion concentrations

Ion chromatographic results showed that the $CH_3SO_3^-$ ion concentration of **1** was 58.5%, which was very close to the calculated value of 57.9%. The sulfate content of **1** was 65 ppm. No halide ions were detected. These results indicated the high purity of the as-prepared protic salt of **1**.

3.2 Thermal, FT-IR and structural analysis

Fig. 1a shows the TG curves of **1**, the n_1/n_2 = 1/3 composition and **2** at a heating rate of 1 K min^{-1}, respectively. The TG curves for **1** and **2** both show a one-step weight loss process. In contrast, the TG curve for the n_1/n_2 = 1/3 composition shows two weight loss events at lower and higher temperatures corresponding to the loss of **2** and **1**, respectively. In addition, the mass ratio of **2** in the n_1/n_2 = 1/3 composition (55.8%) corresponds well with the total weight loss percentage due to the first event (around 56%), indicating a uniform mixture of **1** and **2**. Fig. 1b illustrates that the powder XRD pattern of the n_1/n_2 = 1/3 composition was the combination of those of **1** and **2**, confirming that the crystalline fraction of the **1**/**2** blend was a biphasic mixture of **1** and **2**. This also validates the TG results, proving that no independent third phase exists in the **1**/**2** blend. Hence, as a weaker Brønsted base, **2** is effective to dissolve **1**.

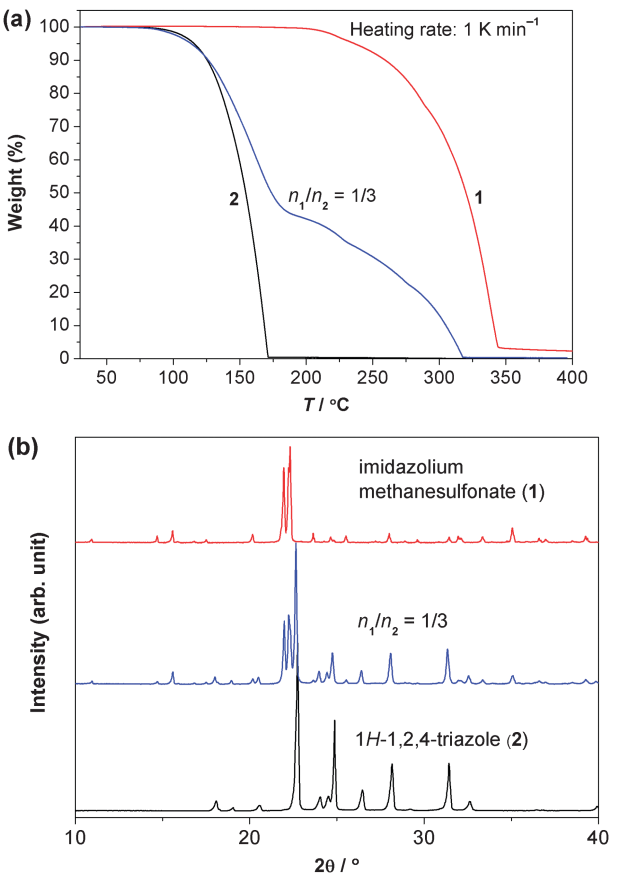

Fig. 1 (a) TG curves and (b) powder XRD patterns of the $C_3H_5N_2^+ \cdot CH_3SO_3^- - C_2H_3N_3$ system, wherein TG and XRD data of **2** are cited from ref. 8.

Table 1 shows T_m and T_e of different compositions. It shows that the melting temperature of **1**/**2** blend was lowered due to the solvation effect of **2**. Notably, **1** has a high T_m of 188.2 °C. As the content of **2** increased, the melting temperature of the **1**/**2** blend decreased remarkably. When the content of **2** increased to n_1/n_2 = 1/3, the blend was observed to have a minimum T_m of 79.5 °C, which is more than 100 K lower than the T_m of **1** and even about 40 K lower than that of **2**. Furthermore, the phase diagram of this binary system is given in Fig. 2. Resembling the simple phase diagrams of choline chloride–urea mixtures[18b] and some other binary systems,[5b,c,8,9,12] the **1**/**2** blend also exhibits a simple eutectic behavior, with a T_e of around 79.5 °C and the eutectic composition at n_1/n_2 = 1/3 (*i.e.* mole fraction of **2** is 0.750). Following the classification of Abbott *et al.*,[18c] the eutectic composition herein may be categorized as the "organic salt + hydrogen bond donor" type of eutectic solvent.

In order to investigate the interactions between **1** and **2**, FT-IR spectra were measured. Fig. 3 shows FT-IR spectra of the $C_3H_5N_2^+ \cdot CH_3SO_3^- - C_2H_3N_3$ system. Obviously, in agreement

Table 1 T_m and T_e of each composition

Composition	x_2[a]	T_m/°C	T_e[b]/°C
1	0	188.2	—
n_1/n_2 = 2/1	0.333	136.4	80.5
n_1/n_2 = 3/4	0.571	86.6	72.6
n_1/n_2 = 1/3	0.750	79.5	79.5
n_1/n_2 = 1/8	0.889	98.2	72.7
2	1	120.4	—

[a] x_2: mole fraction of **2**. [b] For n_1/n_2 = 1/3, only one endothermic peak was observed (T_e = T_m).

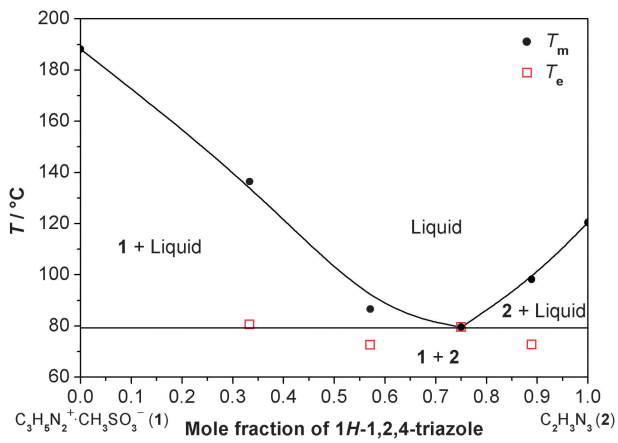

Fig. 2 Phase diagram of the $C_3H_5N_2^+ \cdot CH_3SO_3^- - C_2H_3N_3$ system. The eutectic temperature lies at 79.5 °C.

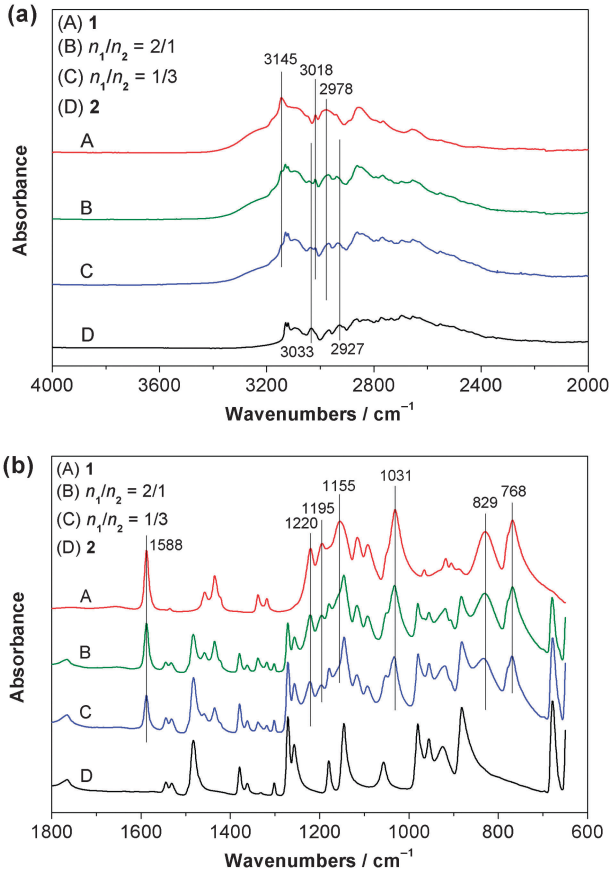

Fig. 3 FT-IR spectra of the $C_3H_5N_2^+ \cdot CH_3SO_3^- - C_2H_3N_3$ system: (a) 2000–4000 cm^{-1}; (b) 650–1800 cm^{-1}, wherein the IR spectrum of **2** is cited from ref. 8.

with the TG and XRD results, the FT-IR spectra of the compositions of n_1/n_2 = 2/1 and n_1/n_2 = 1/3 are on the whole the combination of those of **1** and **2** and thus are further evidence that **2** is solvent for **1**. As displayed in Fig. 3a, the broadening of the bands in the region of 2400–3200 cm^{-1} indicates the system exists in a strongly hydrogen-bonded network.[8,20] The absence of O–H stretching bands between 3400 and 3800 cm^{-1} confirms the very low water contents of the system. Fig. 3b demonstrates that **2** showed almost no change in its spectral feature in the whole system. For example, the peaks at 1483, 1379, 1271, 1257, 1180 and 1146 cm^{-1}, which are associated with the 1*H*-1,2,4-triazole ring stretch,[21] remained at the same position without broadening. This suggests that no protonation of the 1*H*-1,2,4-triazole ring is observable in the system.[8,22] Additionally, no new peak at around 1566 cm^{-1}, associated with the protonation of **2**,[8] was observed. This should be attributed to the fact that imidazole is much more basic than **2**. Particularly, the bands at 3033 and 2927 cm^{-1}, assigned as associated N–H stretching of **2**,[8] shifted to higher wavenumbers once it was mixed with **1**, probably owing to the interaction between **2** and $CH_3SO_3^-$ anion or the separation of molecules of **2** by **1**.

On the other hand, as the content of **2** increased, the bands of **1** got weakened or exhibited somewhat blue shift, reflecting the solvation effect of **2** on **1**. For example, the band at 1588 cm^{-1}, assigned as protonated imidazole ring stretch,[23] became weakened when the content of **2** increased, indicating that **1** was diluted by **2**. So did the bands at 3145 and 1155 cm^{-1}, attributed to aromatic C–H stretching and symmetric ring stretching of **1**,[24] respectively. The peaks at 3018 and 2978 cm^{-1}, most probably related to associated N–H stretching[25] and thus showing the formation of hydrogen bonds in **1**, got weaker or nearly disappeared, suggesting the weakening of hydrogen bonds of **1**. Besides, the bands at 829 and 768 cm^{-1}, associated with the C–H in-plane bend of the imidazolium ring,[24] were both blue-shifted when the content of **2** increased. The presence of hydrogen bonds in imidazolium-based ILs may be indicated by red-shifted C–H frequencies.[20b,26] Inversely, the blue-shifted C–H frequencies probably also demonstrated the weakening of hydrogen bonds of **1** due to the addition of **2**. The peaks at 1220, 1195 and 1031 cm^{-1}, attributed to the SO_3 symmetric or asymmetric stretching vibration of $CH_3SO_3^-$,[8,27] exhibited slight blue shift as **2** increased. In contrast with the reported red shifts of some bands associated with $CH_3SO_3^-$ ions due to the increasing acid–base interactions (*e.g.* CH_3SO_3H–**2**),[8,22] these blue shifts of bands of $CH_3SO_3^-$ ions here indicate the weakening of the electrostatic interactions in **1** due to the solvation effect of **2**. This explains the reduced melting temperature of **1** upon the addition of **2**.

3.3 Computational studies

Proton affinity defines the thermodynamics of proton conduction.[17] Therefore, gas phase proton affinity calculations were performed using density functional theory as implemented in the Gaussian 09 program[28] at the B3LYP/6-311++G(3df,3pd) level.[29–31] The proton affinity of imidazole and **2** were calculated to be 948.8 and 891.4 kJ mol^{-1}, respectively. The calculated proton affinity for imidazole is close to the calculated value of 938.0 kJ mol^{-1} (224.2 kcal mol^{-1}) reported by Subbaraman *et al.*[32] using the Complete Basis Set 4M method. With its lower proton affinity, **2** is expected to stay in the neutral state in the presence of **1**, suggesting that **2** may not function as a proton acceptor but purely acts as a solvent for **1**. This theoretical study supported the TG and FT-IR results.

3.4 Electrochemical behavior

Fig. 4a displays the Arrhenius plots for the ionic conductivity of the system. In the liquid state, the n_1/n_2 = 2/1, n_1/n_2 = 3/4 and n_1/n_2 = 1/3 compositions have almost the same ionic conductivity as **1**, although **2** has a much lower ionic conductivity. The addition of **2** seems to extend the ionic conduction behavior of **1** to a much lower temperature. For example, the ionic conductivity of the n_1/n_2 = 3/4 composition at 90 °C is as high as 0.02 S cm^{-1}. Since the Arrhenius plots indicate that the ionic conductivity exhibits deviation from a simple Arrhenius behavior, the Vogel–Fulcher–Tamman (VFT) equation[2,33,34] shown below was used to analyze the ionic conduction behavior:

$$\sigma(T) = \frac{A}{\sqrt{T}} \exp\left(\frac{-B}{T - T_0}\right) \quad (1)$$

where A is proportional to the concentration of carrier ions, B is the pseudo activation energy for ion conduction, and T_0 is the ideal glass transition temperature.[35] A, B and T_0 were

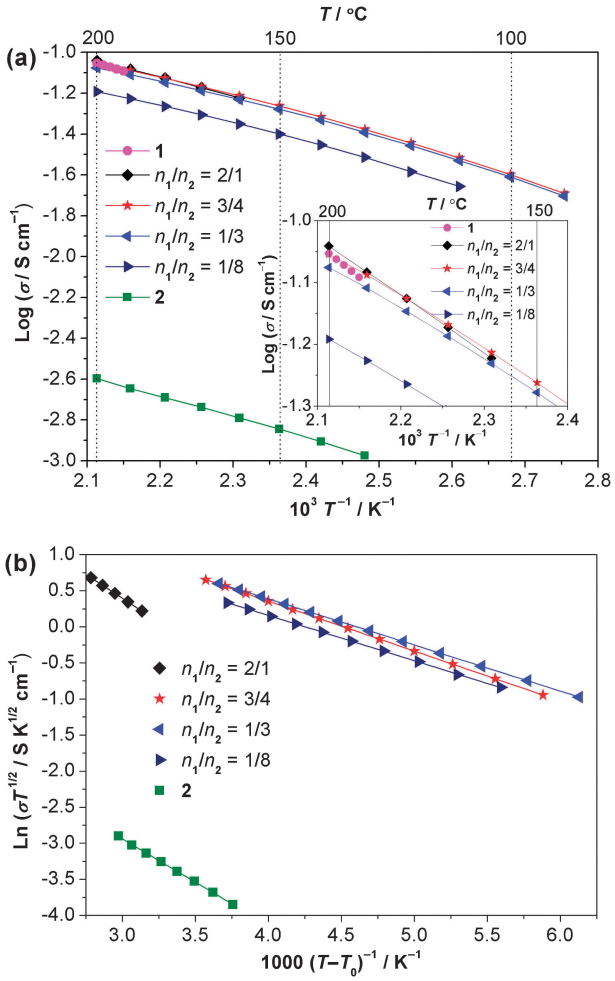

Fig. 4 (a) Arrhenius plots and (b) VFT plots for the ionic conductivity of the $C_3H_5N_2^+ \cdot CH_3SO_3^- - C_2H_3N_3$ system, wherein the data of **2** are cited from ref. 8 and the inset shows an enlarged view of the Arrhenius plots. For VFT plots, the lines represent the VFT fittings.

Table 2 VFT fitting parameters for the ionic conductivity

Composition	A/S K$^{1/2}$ cm^{-1}	B/K	T_0/K	R^{2a}
1[b]	—	—	—	—
n_1/n_2 = 2/1	78.34 ± 32.55	1321 ± 280	114.0 ± 35.7	0.9999
n_1/n_2 = 3/4	22.80 ± 0.45	692.2 ± 8.5	193.1 ± 1.3	0.9999
n_1/n_2 = 1/3	18.95 ± 0.35	638.9 ± 7.8	200.0 ± 1.2	0.9999
n_1/n_2 = 1/8	14.49 ± 0.90	628.6 ± 27.0	204.3 ± 4.6	0.9999
2	1.949 ± 0.752	1202 ± 230	136.9 ± 28.3	0.9998

[a] R^2: correlation coefficient. [b] For **1**, minimized deviation from the VFT equation could not be reached, probably due to limited points of ionic conductivity data and the narrow temperature region (192–200 °C). The fitting result of **2** is adopted from ref. 8.

all adjustable parameters. The best-fit parameters, which minimize the deviation from the VFT equation,[8,35] are tabulated in Table 2. The VFT plots are demonstrated to be straight lines in Fig. 4b. Obviously, the ionic conductivity of the system follows the prediction of the VFT equation very well.

Furthermore, since no protonation of **2** was observed in Fig. 3b and **2** may not function as a proton acceptor for **1**, the Grotthuss mechanism is unlikely to dominate the proton conduction. Therefore, the vehicle mechanism[4,36,37] should mainly govern the proton conduction for the system containing **1**, likely in the form of imidazolium cation. From the n_1/n_2 = 2/1 composition to pure **2**, the decreasing values of A shown in Table 2 confirm that the addition of **2** to **1** decreased the carrier ion concentration. It is well-known that the ionic conductivity of amorphous materials depends on both carrier ion concentration and mobility. Based on the simulation model for proton transport in liquid imidazole by Voth *et al.*,[38] it is speculated that ordered solvation shells of **2** are formed around the ions while the ion concentration of **1** is decreased upon the addition of **2**. One reason for why the high ionic conductivity of **1** was maintained in a wide composition range while the melting temperature decreased gradually and the carrier ion concentration was reduced is suggested as follows: as the electrostatic interactions between the cation and the anion of the PIL are expected to cause a decrease in mobility,[1a] the addition of the neutral molecules of **2** weakens the electrostatic interactions through the solvation shells which separate cation–anion packing interactions,[39] hence increasing the mobility of ions and lowering the melting temperature. The Nernst–Einstein equation for 1 : 1 electrolytes[40] is also applied to interpret the increased mobility:

$$\sigma = \frac{cF^2}{RT}(D_{\text{cation}} + D_{\text{anion}}) \qquad (2)$$

where c is the molar concentration of the electrolyte, F the Faraday constant, R the gas constant, and T the absolute temperature. As the molar concentration of **1** decreased dramatically upon the addition of **2**, a relatively constant ionic conductivity at the same temperature indicated that the ionic diffusion coefficients (D_{cation} and D_{anion}) would increase sufficiently. In another word, the effect of reduced carrier ion concentration was compensated by the enhanced ionic mobility, resulting in similar ionic conductivities in the liquid state for these compositions. This also implies that as a solvent, **2** effectively dissociated **1**.

Fig. 5a shows chronoamperograms of the n_1/n_2 = 1/3 composition at 150 °C as a representative case for the **1**/**2** blend at an applied potential of 500 mV. The current detected under N_2 atmosphere promptly attenuated to nearly zero within a few seconds, suggesting the formation of an electric double layer.[19,41] Conversely, a significant and stable current was observed under a H_2 atmosphere. Furthermore, evolution of gas bubbles (H_2) was visually confirmed at the cathode. Therefore, the following processes occurred in the electrochemical cell consisting of the three-electrode system and the electrolyte:

$$\text{Anode (WE): } H_2 + 2C_3H_4N_2 \rightarrow 2C_3H_5N_2^+ + 2e^-$$

$$\text{Electrolyte: } H^+ \text{ conduction from anode to cathode}$$

$$\text{Cathode (CE): } 2C_3H_5N_2^+ + 2e^- \rightarrow 2C_3H_4N_2 + H_2$$

Fig. 5b presents the cyclic voltammograms at 20 mV s^{-1} for the n_1/n_2 = 1/3 composition at 150 °C under dry H_2, N_2 and O_2 atmosphere, respectively. When the WE was in a N_2 atmosphere, the voltammograms showed remarkable reduction current (also notable oxidation current when the scan rate was 100 mV s^{-1}) at around 0 V. Meanwhile, gas bubbles were observed on the WE during the reduction

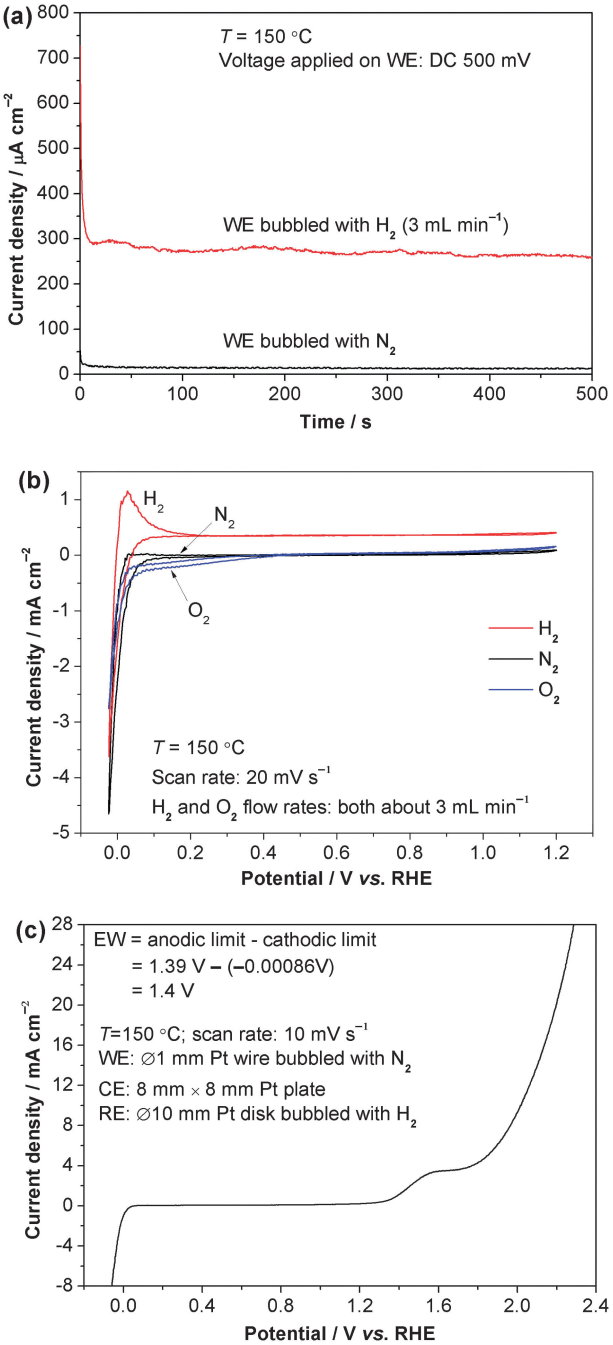

Fig. 5 (a) Chronoamperograms for $n_1/n_2 = 1/3$ under dry H_2 or N_2 atmosphere at 150 °C, (b) cyclic voltammograms for $n_1/n_2 = 1/3$ under dry H_2, N_2 or O_2 atmosphere, and (c) linear sweep voltammogram for $n_1/n_2 = 1/3$ under a dry N_2 atmosphere.

process at around 0 V. The potential of 0 V, therefore, corresponds to the hydrogen redox potential in this electrolyte, and the RE can be considered as a RHE.[3] Upon switching to a H_2 atmosphere, large oxidation currents were detected due to the steady-state H_2 oxidation on the WE:

$$H_2 + 2C_3H_4N_2 \rightarrow 2C_3H_5N_2^+ + 2e^-$$

The formation of bubbles was also visible on the CE. Evolution of hydrogen gas was the only possible explanation for this observation which confirmed the proton conduction for the **1**/**2** blend. When the WE was under an O_2 atmosphere, a distinct change in the shape of the voltammograms was observed. A cathodic current was observed at a potential below 0.5 V *vs.* RHE, indicating oxygen reduction. The waves, corresponding to the evolution and reoxidation of H_2, appeared around 0 V *vs.* RHE. The high overpotential for the oxygen reduction reaction in imidazolium-based PILs has been described earlier.[3,9] The reaction might be:

$$O_2 + 4C_3H_5N_2^+ + 4e^- \rightarrow 4C_3H_4N_2 + 2H_2O$$

Fig. 5c shows the linear sweep voltammogram for the $n_1/n_2 = 1/3$ composition obtained at 150 °C under a N_2 atmosphere with a sweep rate of 10 mV s^{-1}. The electrochemical window (EW), which is defined as the potential range where the reduction and oxidation current densities both remain within 1.0 mA cm^{-2}, was 1.4 V for the $n_1/n_2 = 1/3$ composition, indicating that the **1**/**2** blend is electrochemically stable under PEMFC conditions and therefore could be potentially used as electrolytes for PEMFCs under non-humidifying conditions. At present, we are not clear of the reason for the rising current beginning at around 1.25 V *vs.* RHE. Nevertheless, Liu *et al.* reported a large irreversible oxidation peak near +1.0 V (*vs.* Ag/Ag^+) in the voltammogram for imidazole in CH_3CN solution, showing the poisoning effect of imidazole.[11] Considering that the EWs of **2** and 1,2,4-triazolium methanesulfonate were 2.1 V and 2.0 V,[8] respectively, the observed rising current might be attributed to the imidazolium cation moiety in **1**.

4. Conclusions

The solvation effect of 1*H*-1,2,4-triazole (**2**) towards imidazolium methanesulfonate (**1**) was investigated. It was found that **2** was effective to dissolve and dissociate **1**. FT-IR spectra revealed the weakening of electrostatic interactions and hydrogen bonds of **1** while no protonation of **2** was observed. While the addition of **2** evidently lowered the melting temperatures, the high ionic conductivity of **1** was maintained for a wide composition range. The ionic conductivity of the whole system followed the prediction of the VFT equation very well. The proton mobility seemed to obey the vehicle mechanism with an imidazolium cation as a vehicle for the system containing **1**. Proton conduction has been verified. The **1**/**2** blend exhibited electrochemical activities for H_2 oxidation and O_2 reduction at a Pt electrode. The system under study showed an adequate electrochemical window for PEMFC application.

Acknowledgements

The authors gratefully acknowledge technical discussions about DSC data with Prof. Dr Christ Glorieux (KU Leuven), Dr Jan Leys (KU Leuven), Dr Juergen Blumm (NETZSCH-Gerätebau GmbH) and Dr Stéphane Longuemart (Université du Littoral Côte d'Opale). We thank Dr Martin Knipper (Universität Oldenburg) for the help with powder XRD measurements. J.L. and I.F.J.V. acknowledge IOF-KP 10/005 of

KU Leuven for financial support. J.L. deeply thanks Prof. Dr Carsten Agert and Dr Alexander Dyck (NEXT ENERGY) for the opportunity to conduct the experimental work at NEXT ENERGY and gratefully acknowledges their financial support. The authors are grateful to the reviewers for their valuable comments and suggestions, which greatly improved the quality of this manuscript.

Notes and references

1 (*a*) T. L. Greaves and C. J. Drummond, *Chem. Rev.*, 2008, **108**, 206; (*b*) M. Armand, F. Endres, D. R. MacFarlane, H. Ohno and B. Scrosati, *Nat. Mater.*, 2009, **8**, 621; (*c*) J. Snyder, T. Fujita, M. W. Chen and J. Erlebacher, *Nat. Mater.*, 2010, **9**, 904; (*d*) Y. Tan, C. Xu, G. Chen, N. Zheng and Q. Xie, *Energy Environ. Sci.*, 2012, **5**, 6923.
2 H. Ohno and M. Yoshizawa, *Solid State Ionics*, 2002, **154–155**, 303.
3 M. A. B. H. Susan, A. Noda, S. Mitsushima and M. Watanabe, *Chem. Commun.*, 2003, 938.
4 H. Nakamoto and M. Watanabe, *Chem. Commun.*, 2007, 2539.
5 (*a*) J.-P. Belieres and C. A. Angell, *J. Phys. Chem. B*, 2007, **111**, 4926; (*b*) J.-P. Belieres, D. Gervasio and C. A. Angell, *Chem. Commun.*, 2006, 4799; (*c*) Z. Zhao, K. Ueno and C. A. Angell, *J. Phys. Chem. B*, 2011, **115**, 13467.
6 (*a*) F. Yan, S. Yu, X. Zhang, L. Qiu, F. Chu, J. You and J. Lu, *Chem. Mater.*, 2009, **21**, 1480; (*b*) C. Zhao, G. Burrell, A. A. J. Torriero, F. Separovic, N. F. Dunlop, D. R. MacFarlane and A. M. Bond, *J. Phys. Chem. B*, 2008, **112**, 6923.
7 H. Nakamoto, A. Noda, K. Hayamizu, S. Hayashi, H.-O. Hamaguchi and M. Watanabe, *J. Phys. Chem. C*, 2007, **111**, 1541.
8 J. Luo, J. Hu, W. Saak, R. Beckhaus, G. Wittstock, I. F. J. Vankelecom, C. Agert and O. Conrad, *J. Mater. Chem.*, 2011, **21**, 10426.
9 A. Noda, M. A. B. H. Susan, K. Kudo, S. Mitsushima, K. Hayamizu and M. Watanabe, *J. Phys. Chem. B*, 2003, **107**, 4024.
10 K. M. Johansson, E. I. Izgorodina, M. Forsyth, D. R. MacFarlane and K. R. Seddon, *Phys. Chem. Chem. Phys.*, 2008, **10**, 2972.
11 S. Li, Z. Zhou, Y. Zhang, M. Liu and W. Li, *Chem. Mater.*, 2005, **17**, 5884.
12 K. D. Kreuer, A. Fuchs, M. Ise, M. Spaeth and J. Maier, *Electrochim. Acta*, 1998, **43**, 1281.
13 L. Timperman, H. Galiano, D. Lemordant and M. Anouti, *Electrochem. Commun.*, 2011, **13**, 1112.
14 M. Anouti, A. Vigeant, J. Jacquemin, C. Brigouleix and D. Lemordant, *J. Chem. Thermodyn.*, 2010, **42**, 834.
15 K. A. Kurnia, M. I. A. Mutalib, T. Murugesan and B. Ariwahjoedi, *J. Solution Chem.*, 2011, **40**, 818.
16 W. L. F. Armarego and C. L. L. Chai, *Purification of Laboratory Chemicals*, Butterworth-Heinemann, Oxford, 6th edn, 2009.
17 R. Subbaraman, H. Ghassemi and T. A. Zawodzinski Jr., *J. Am. Chem. Soc.*, 2007, **129**, 2238.
18 (*a*) C. A. Angell, W. Xu, J.-P. Belieres and M. Yoshizawa, *Patent WO*114445, 2004; (*b*) A. P. Abbott, G. Capper, D. L. Davies, R. K. Rasheed and V. Tambyrajah, *Chem. Commun.*, 2003, 70; (*c*) A. P. Abbott, G. Capper and S. Gray, *ChemPhysChem*, 2006, **7**, 803.
19 T. Mizumo, T. Watanabe and H. Ohno, *Polym. J. (Tokyo)*, 2008, **40**, 1099.
20 (*a*) A. Aslan, S. Ü. Çelik, Ü. Şen, R. Haser and A. Bozkurt, *Electrochim. Acta*, 2009, **54**, 2957; (*b*) A. Elaiwi, P. B. Hitchcock, K. R. Seddon, N. Srinivasan, Y.-M. Tan, T. Welton and J. A. Zora, *J. Chem. Soc., Dalton Trans.*, 1995, 3467.
21 F. Billes, H. Endrédi and G. Keresztury, *THEOCHEM*, 2000, **530**, 183.
22 S. Guhathakurta and K. Min, *Polymer*, 2009, **50**, 1034.
23 D. H. Bonsor, B. Borah, R. L. Dean and J. L. Wood, *Can. J. Chem.*, 1976, **54**, 2458.
24 P. B. Hitchcock, K. R. Seddon and T. Welton, *J. Chem. Soc., Dalton Trans.*, 1993, 2639.
25 S. Tait and R. A. Osteryoung, *Inorg. Chem.*, 1984, **23**, 4352.
26 (*a*) A. Wulf, K. Fumino and R. Ludwig, *Angew. Chem., Int. Ed.*, 2010, **49**, 449; (*b*) C. M. Burba, N. M. Rocher and R. Frech, *J. Phys. Chem. B*, 2009, **113**, 11453.
27 R. Langner and G. Zundel, *J. Chem. Soc., Faraday Trans.*, 1998, **94**, 1805.
28 M. J. Frisch, G. W. Trucks, H. B. Schlegel, G. E. Scuseria, M. A. Robb, J. R. Cheeseman, G. Scalmani, V. Barone, B. Mennucci, G. A. Petersson, H. Nakatsuji, M. Caricato, X. Li, H. P. Hratchian, A. F. Izmaylov, J. Bloino, G. Zheng, J. L. Sonnenberg, M. Hada, M. Ehara, K. Toyota, R. Fukuda, J. Hasegawa, M. Ishida, T. Nakajima, Y. Honda, O. Kitao, H. Nakai, T. Vreven, J. A. Montgomery Jr, J. E. Peralta, F. Ogliaro, M. Bearpark, J. J. Heyd, E. Brothers, K. N. Kudin, V. N. Staroverov, R. Kobayashi, J. Normand, K. Raghavachari, A. Rendell, J. C. Burant, S. S. Iyengar, J. Tomasi, M. Cossi, N. Rega, J. M. Millam, M. Klene, J. E. Knox, J. B. Cross, V. Bakken, C. Adamo, J. Jaramillo, R. Gomperts, R. E. Stratmann, O. Yazyev, A. J. Austin, R. Cammi, C. Pomelli, J. W. Ochterski, R. L. Martin, K. Morokuma, V. G. Zakrzewski, G. A. Voth, P. Salvador, J. J. Dannenberg, S. Dapprich, A. D. Daniels, Ö. Farkas, J. B. Foresman, J. V. Ortiz, J. Cioslowski and D. J. Fox, *Gaussian 09, Revision A.2*, Gaussian, Inc, Wallingford, CT, 2009.
29 C. Lee, W. Yang and R. G. Parr, *Phys. Rev. B: Condens. Matter Mater. Phys.*, 1988, **37**, 785.
30 A. D. Becke, *J. Chem. Phys.*, 1993, **98**, 5648.
31 P. J. Stephens, F. J. Devlin, C. F. Chabalowski and M. J. Frisch, *J. Phys. Chem.*, 1994, **98**, 11623.
32 R. Subbaraman, H. Ghassemi and T. Zawodzinski Jr., *Solid State Ionics*, 2009, **180**, 1143.
33 (*a*) H. Vogel, *Phys. Z.*, 1921, **22**, 645; (*b*) G. S. Fulcher, *J. Am. Ceram. Soc.*, 1925, **8**, 339; (*c*) G. Tamman and W. Z. Hesse, *Z. Anorg. Allg. Chem.*, 1926, **156**, 245.
34 C. A. Angell, *J. Phys. Chem.*, 1964, **68**, 1917.
35 S. Seki, M. A. B. H. Susan, T. Kaneko, H. Tokuda, A. Noda and M. Watanabe, *J. Phys. Chem. B*, 2005, **109**, 3886.
36 J. W. Blanchard, J.-P. Belières, T. M. Alam, J. L. Yarger and G. P. Holland, *J. Phys. Chem. Lett.*, 2011, **2**, 1077.
37 M. Yoshizawa and H. Ohno, *Chem. Commun.*, 2004, 1828.
38 H. Chen, T. Yan and G. A. Voth, *J. Phys. Chem. A*, 2009, **113**, 4507.
39 J. D. Holbrey, W. M. Reichert, M. Nieuwenhuyzen, O. Sheppard, C. Hardacre and R. D. Rogers, *Chem. Commun.*, 2003, 476.
40 H. Weingärtner, *Angew. Chem., Int. Ed.*, 2008, **47**, 654.
41 (*a*) M. V. Fedorov, N. Georgi and A. A. Kornyshev, *Electrochem. Commun.*, 2010, **12**, 296; (*b*) F. Endres, O. Höfft, N. Borisenko, L. H. Gasparotto, A. Prowald, R. Al-Salman, T. Carstens, R. Atkin, A. Bund and S. Z. E. Abedin, *Phys. Chem. Chem. Phys.*, 2010, **12**, 1724; (*c*) R. M. Lynden-Bell, A. I. Frolov and M. V. Fedorov, *Phys. Chem. Chem. Phys.*, 2012, **14**, 2693; (*d*) R. Hayes, G. G. Warr and R. Atkin, *Phys. Chem. Chem. Phys.*, 2010, **12**, 1709; (*e*) F. Endres, N. Borisenko, S. Z. E. Abedin, R. Hayes and R. Atkin, *Faraday Discuss.*, 2012, **154**, 221; (*f*) X. Si, S. Li, Y. Wang, S. Ye and T. Yan, *ChemPhysChem*, 2012, **13**, 1671; (*g*) A. A. Kornyshev, *J. Phys. Chem. B*, 2007, **111**, 5545; (*h*) M. Z. Bazant, B. D. Storey and A. A. Kornyshev, *Phys. Rev. Lett.*, 2011, **106**, 046102.